Heat Treatment of Hydrogen Molybdenum Bronze in an Oxygen-Free Atmosphere. Formation of a Defect Structure and Attempt to Carry Out a Catalytic Reaction

Kentaro Nakamura,* Kazuo Eda, and Noriyuki Sotani*

Department of Chemistry, Faculty of Science, Kobe University, Nada, Kobe 657-8501

(Received February 20, 1998)

Hydrogen molybdenum bronze, H_xMoO_3 ($x = 0.25$), was treated in vacuo, which was changed by four steps to form MoO_3 and MoO_2 through the Type-I and the MoO_3-like structure with defects, such as an oxygen vacancy. The structural changes were studied by TG-DTA, XRD, ESR, and XANES. Type-I with a defect structure was effective for the isomerization of 1-butene.

Generally, hydrogen molybdenum bronze, H_xMoO_3 ($0 < x \leqq 2$), shows a metallic conductivity and is expected to be used for a battery electrode, a proton conductor, a catalyst and so on. It is obtained by introducing hydrogen into MoO_3 in an acidic media or by hydrogen spillover.[1—6] Four distinct phases have been confirmed in the region of homogeneity with an approximate limit: Type-I (blue, orthorhombic, $0.21 \leqq x \leqq 0.4$); Type-II (blue, monoclinic, $0.85 \leqq x \leqq 1.04$); Type-III (red, monoclinic, $1.55 \leqq x \leqq 1.72$); Type-IV (green, monoclinic, $1.95 \leqq x \leqq 2.0$).[4,7] Among them, Type-I has been characterized by many authors using X-ray diffraction,[4] neutron diffraction,[8] thermal decomposition,[9—11] IR,[3,12,13] and NMR.[5,14] Upon heating, the hydrogen in the bronze is known to be released in two ways. One is in an oxygen-free atmosphere, such as[1,3,11,15]

$$H_xMoO_3 \longrightarrow \frac{x}{2}H_2O + MoO_{3-x/2}. \quad (1)$$

The other is in air, such as

$$H_xMoO_3 \longrightarrow \frac{x}{2}H_2 + MoO_3. \quad (2)$$

By the former way (1), a defect structure may be produced by removing H_2O, which is produced by connecting with hydrogen and the lattice oxygen in a nitrogen atmosphere or in vacuo. It is well known that MoO_3 gives a Magneli phase by reduction, such as Mo_nO_{3n-1} and/or Mo_nO_{3n-2} including Mo^{5+} ion, which has a share structure, called a Magneli dislocation. Type-I is expected to produce the Magneli phase upon heating in vacuo. Indeed, Eda[16] studied the thermal decomposition of Type-I in a nitrogen atmosphere and discussed the decomposition mechanism. He proposed that the decomposition took place by two processes. One is a low-temperature process, which produces MoO_2 through a defect structure. The order is a high-temperature process, which produces Mo_4O_{11}, one of the Magneli phase, via another defect structure. In this work, we studied the structural change of Type-I and the formation of a defect structure. The precise mechanism for thermal decomposition in an oxygen-free atmosphere is discussed. Type-I with a defect structure is expected to be useful for a catalytic reaction. Therefore, we tried to use this sample as a catalyst for the isomerization of 1-butene. Since it showed a catalytic activity, we considered the active site.

Experimental

Sample Preparation. The preparation of hydrogen molybdenum bronze, H_xMoO_3, was described previously.[1,9—11] The hydrogen content was determined by thermogravimetry[11] and by Choain and Marion's method.[17] It was determined to be $x = 0.25$, which was identical with Type-I having an orthorhombic structure according to XRD. Afterward, we call this "Type-I".

Characterization. TG-DTA result was obtained by a MAC Science TG-DTA 2000S under nitrogen flow. The sample was examined by the powder X-ray diffraction (XRD) method using a Rigaku RINT 1200 X-ray diffractomator. The BET surface area, SA; $m^2\,g^{-1}$, of the samples was determined from the nitrogen-adsorption isotherm at 77 K using a QUANTASORB Jr. (Quantachrome Co.). The behavior of paramagnetic species in the catalyst was studied using a JEOL ESR with an X-band at the liquid-nitrogen temperature. The g-value was determined by using a Mn^{2+} marker as a reference. The Mo L_3-edge absorption XANES, X-ray Absorption Near Edge Structure, spectra were measured on BL-7A of UVSOR at the Institute for Molecular Science, Okazaki, Japan, using a Ge (111) two-crystal monochromator. The experimental method was described elsewhere.[18]

Catalytic Reaction. A catalytic reaction was carried out at 373 K in a closed gas-circulation system. The catalyst (200 mg) was loaded into the glass reaction tube, which was treated at various temperatures for 1 h before use. After being cooled down to room temperature, 1-butene (Tokyo Kasei, 200 Torr) was introduced into the reaction vessel. The products were analyzed by a Yanaco G2800T Gas Chromatograph, which was connected directly to the

gas-circulation system.

Results and Discussion

Heat Treatment of Type-I in an Oxygen-Free Atmosphere. Figure 1 shows a DTA curve in a nitrogen atmosphere of Type-I, which gives three endothermic peaks with weight loss. The peak at 380 K was accompanied by a small weight loss (0.04 wt%) resulting from dehydration of the physically adsorbed water. A very broad peak appeared at from 500 to 650 K along with a gradual weight decrease by 0.81 wt%. The peak at 664 K showed a sharp change accompanied by rapid weight loss of 0.71 wt%. This suggests two kinds of dehydrogenation processes. When Type-I was heated in vacuo, according to the XRD results, MoO_2 began to appear at 573 K and MoO_3, at 673 K. The component consisted of Type-I below 573 K, of a mixture of Type-I, MoO_2 and MoO_3 at the temperature between 573 and 673 K, and of MoO_2 and MoO_3 above 673 K, as shown in Fig. 2. The relative intensities of Type-I, MoO_2, and MoO_3 were plotted against the treated temperature in Fig. 3, which were calculated from the maximum diffraction peak heights of each component, as shown by the arrow in Fig. 2. The intensity of Type-I was kept constant up to around 523 K, began to decrease monotonously, and then disappeared completely above 773 K. On the other hand, MoO_2 began to appear at 573 K, and the intensity gradually increased. MoO_3 began to appear at 673 K. The intensity increased sharply to 723 K, and then gradually increased above 723 K. Above 673 K the intensity of MoO_3 was about 2.5-times that of MoO_2.

Figure 4 shows the BET surface areas (SA) of Type-I treated at various temperatures in vacuo. SA of the original Type-I was 3.5 $m^2 g^{-1}$. This was larger than that of MoO_3 (1.2 $m^2 g^{-1}$) by about three times, which was obtained from Type-I by heating in air at about 800 K. SA gave no significant change until 623 K. However, it began to increase at 623 K, took a maximum (5.0 $m^2 g^{-1}$) at around 723 K, and then decreased to a slightly smaller value compared to that of the original Type-I. The increase in SA just corresponds to the steep increase in MoO_3 up to 723 K, which may contain a distorted defect structure.

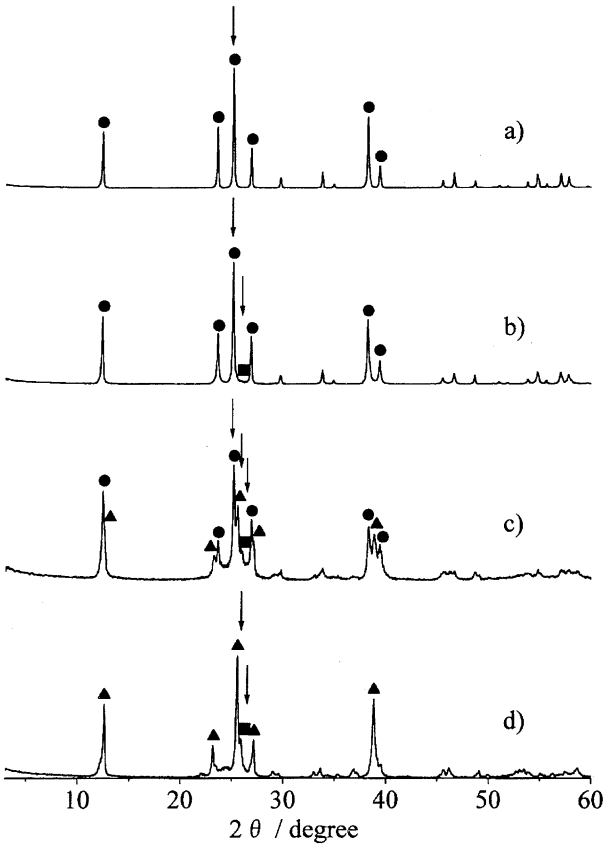

Fig. 2. XRD patterns of Type-I treated in vacuo at a) room temperature —523 K, b) 573—623 K, c) 673—693 K, and d) 723—873 K. Symbols of ●, ■, and ▲ represent Type-I, MoO_2, and MoO_3, respectively. The arrows represent the XRD peaks which are used in the calculation for the intensity.

Paramagnetic Property of Type-I. Type-I was studied by ESR to reveal the paramagnetic character. ESR studies on the Mo ion give us very important information about the coordination state and the ligand field. Type-I before use gave

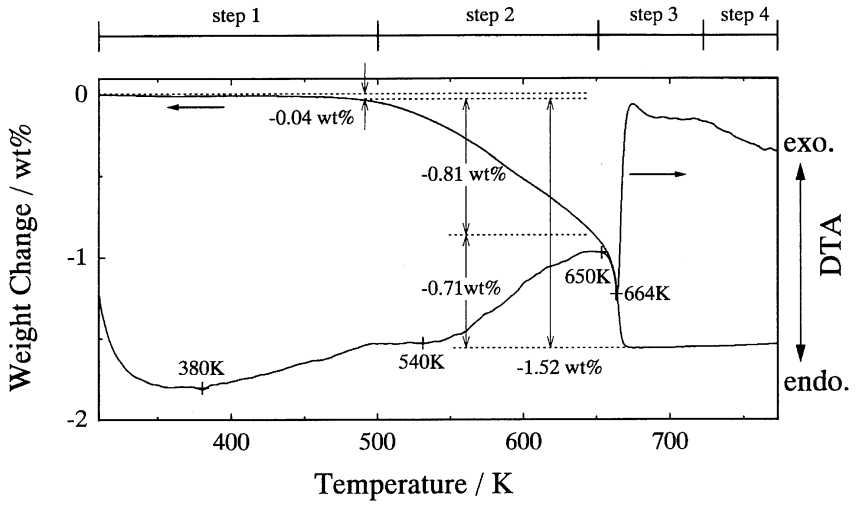

Fig. 1. TG-DTA curve of Type-I in nitrogen atmosphere.

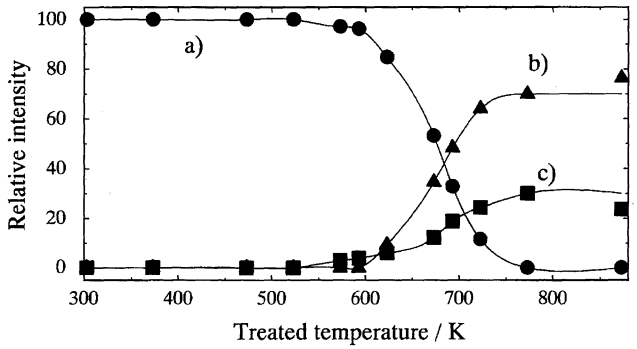

Fig. 3. Change in the relative XRD diffraction intensity ratio of a) Type-I, ●, b) MoO_3, ▲, and c) MoO_2, ■.

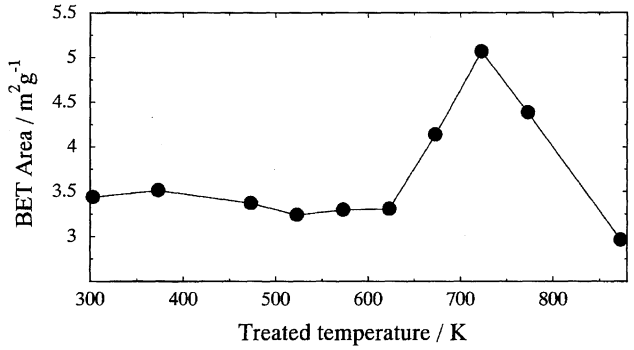

Fig. 4. Change in Specific surface area of Type-I treated at various temperatures in vacuo.

no ESR signal at room temperature. Figure 5 shows typical ESR spectra of Type-I treated at several temperatures in vacuo, which were observed at liquid-nitrogen temperature. When Type-I was treated at from room temperature to 523 K, the spectrum gave a good symmetry with a g-value at 1.939 (the top of signal has g=1.946). From 573 to 623 K, the spectrum was antisymmetric and very complicated. Signals with g=1.946, 1.924, and 1.883 were clearly observed. From 673 to 693 K, the spectrum was a little noisy and became broad at the high magnetic-field side. The spectrum looks like a broad single signal, but it may contain several signals. Although type-I treated at from 723 to 873 K showed a smooth single symmetric-like spectrum, but a doublet at around g=1.94 was observed.

The third-derivative curve of the spectrum gives important information concerning the g-value. Figure 6 shows the third derivative of the spectrum at 873 K, which, in fact, comprises several signals. The third derivative of the spectrum at 873 K gave g-values at 2.003, 1.946, 1.938, 1.924, 1.899, and 1.883. The obtained g-values from the third derivative are summarized in Table 1. We tried to assign the ESR signals observed in this study. Mo ion can exist in one of four valence states, 6+, 5+, 4+, and 3+, corresponding to the d^0, d^1, d^2, and d^3 configurations. Mo^{6+} is diamagnetic and, therefore, gives no ESR signal. Mo^{4+}, even though it is paramagnetic, can be observed only at very low temperature. Since the resonance due to d^2 would have a large zero-field splitting, it would give a very broad signal.[19,20] Indeed, in our experience, the signal due to Mo^{4+} has not been observed. By

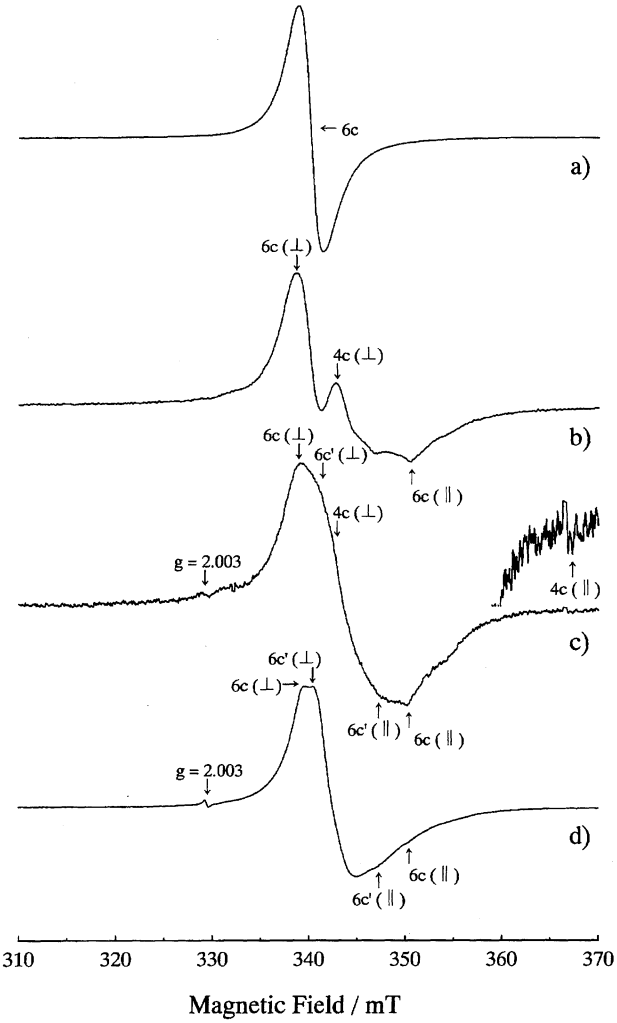

Fig. 5. ESR spectra of Type-I treated in vacuo at a) room temperature —523 K, b) 573—623 K, c) 673—693 K, and d) 723—873 K.

considering the above-mentioned reasons, the observed signals must be due to Mo^{5+} and Mo^{3+}. Several ESR studies of Mo^{3+} have been reported. Griffiths, Owen, and Ward[21] have reported isotropic g-values of around 1.96 for hydrated and unhydrated chloro and fluoro complexes of Mo^{3+}. Dyrek and Labanowska also observed Mo^{3+} in polycrystalline MoO_3 at around g=1.978.[22] However, under our experimental conditions, Mo^{6+} is hard to be reduced to Mo^{3+} and XRD results give no compound which consists of Mo^{3+}. Therefore, all signals should have resulted from Mo^{5+}. The assignments of the signal due to Mo^{5+} under several conditions have already been proposed by many workers.[18,22,24—27]

At the second step, Type-I changes to $H_{0.11}MoO_{2.93}$, which lacks oxygen, because the inserted protons are removed as H_2O by connecting with the lattice oxygen. According to XRD results, the sample mostly keeps the Type-I structure. This indicates the formation of a defect structure like an oxygen vacancy. Therefore, the signal at g=2.003 should be assigned to a defect structure like an oxygen vacancy.[18,22,23] Che et al.[26] proposed three Mo^{5+} species, which were assigned to the tetra-, penta-, and hexa-coordinated species. According

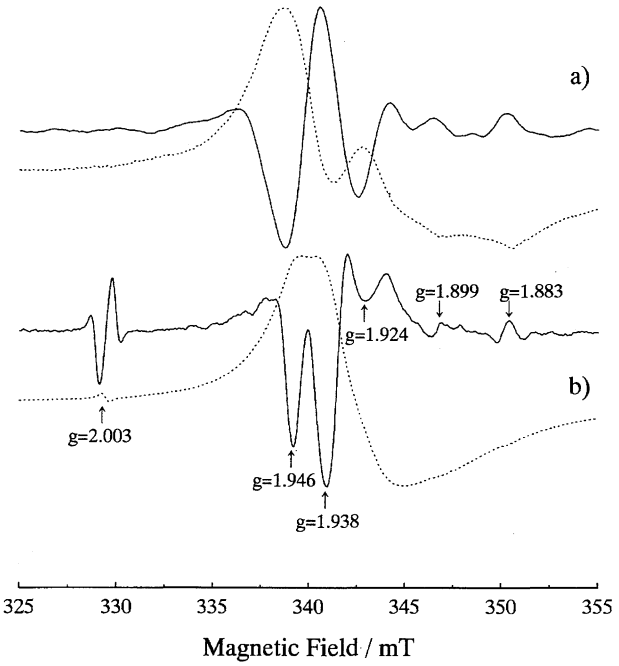

Fig. 6. The third derivatives of ESR spectra of Type-I treated in vacuo at a) 573 K and b) 873 K. Solid and dashed lines represent the third derivatives and the original spectra, respectively.

to Che et al. and other workers, $g=1.956$ was assigned to the vertical component ($g_\perp$) of penta-coordinated Mo^{5+} ion (Mo^{5+}_{5c}),[18,22,24—27] $g=1.941$—1.943 to $g_\perp$ of hexa-coordinated Mo^{5+} ion (Mo^{5+}_{6c}),[18,22,24—27] and $g=1.927$ to $g_\perp$ of tetra-coordinated Mo^{5+} ion (Mo^{5+}_{4c}),[18,22,24—27] respectively. The signal at $g=1.893$, 1.870—1.879, and 1.778 was assigned to the parallel component ($g_{//}$) of the hexa-, penta-, and tetra-coordinated Mo^{5+} ion, respectively.[18,22,24—27] As shown in Fig. 6, the spectrum of 873 K clearly shows two distinct g-values at 1.946 and 1.938. We assigned the signal at around $g=1.94$ obtained from the MoO_3–ZnO catalyst to the vertical component ($g_\perp$) of hexa-coordinate Mo^{5+} resulting from a lack of one vertex oxygen which constructs a MoO_6 octahedron.[18] Accordingly, the signal at $g=1.946$ can be assigned to the vertical component of the hexa-coordinate Mo^{5+}. A signal with $g=1.938$ appeared above 673 K. According to previous workers,[18,22,24—27] the signal with $g=1.938$ was different from the hexa-coordinate Mo^{5+} proposed by Che et al.[26] However this is assigned to the vertical component due to the hexa-coordinate Mo^{5+} ($Mo^{5+}_{6c'}$) in a rhombically distorted MoO_6 octahedron. According to the XRD results, MoO_3 appeared. The composition is $MoO_{2.87}$ based on a chemical analysis, and SA increases. Therefore, the MoO_3-like structure with a defect structure should be formed and a MoO_6 octahedron with the defect may be distorted. The signal at $g=1.938$ becomes clear at high temperature. Therefore, it is reasonable that the signal with $g=1.938$ is due to a distorted MoO_6 octahedron with a defect. On the other hand, when the sample was treated at around 573 K, a signal at $g=1.924$ was observed. At around these temperature ranges MoO_2 began to appear. Eda[16] proposed that, along with MoO_2, a shear structure should be formed. The shear structure along the boundary of MoO_2 might contain a tetrahedron with a defect. This gave a signal at $g=1.927$ due to the vertical component of the tetra-coordinate Mo^{5+} ion (Mo^{5+}_{4c}).[18] In this study, it is reasonable to assign the signal at $g=1.924$ to tetrahedral coordinated Mo^{5+} ion (Mo^{5+}_{4c}).[18,22,24—27] The signals at $g=1.899$, 1.883, and 1.778 are due to the parallel components ($g_{//}$) of 6c, 6c′ and 4c, respectively.[18,22,24—27] These g-values and assignments are summarized in Table 1.

The relative intensity of the ESR signals of Type-I treated at various temperatures in vacuo is shown in Fig. 7, which is calculated from the integrated area of the spectrum by comparing it with one of the first standard Mn^{2+}. The relative intensity contains the total amount of radicals in the sample. Most of the component is due to Mo^{5+}, because another component due to the signal at $g=2.003$ is very small compared to that of Mo^{5+}. However, it is very difficult to clarify each Mo^{5+} component. The intensity gradually increased at

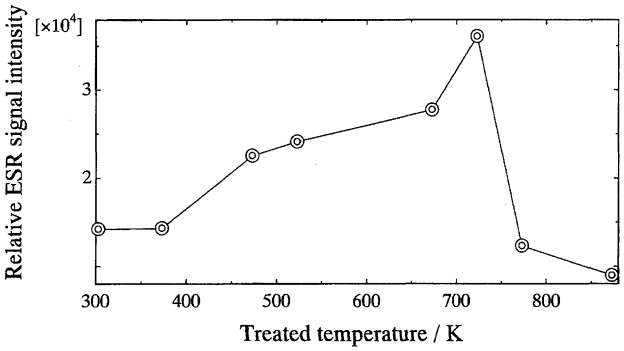

Fig. 7. Change in the total relative intensity ratio of ESR signal of Type-I treated at various temperatures in vacuo.

Table 1. The g-Values of the ESR Signals Observed on Type-I

	Treated temperature				Assignment	Reference
	R.T.	573 K	673 K	873 K		
	—	—	2.003	2.003	Lattice defect site	21—23
	1.946	1.946	1.946	1.946	$g_\perp$ component of hexa-coodinated Mo^{5+} (Mo^{5+}_{6c})	18, 22, 24—27
	—	—	1.938	1.938	$g_\perp$ component of hexa-coordinated Mo^{5+} ($Mo^{5+}_{6c'}$)	18, 22, 24—27
g-Value	—	1.924	1.924	1.924	$g_\perp$ component of tetra-coordinated Mo^{5+} (Mo^{5+}_{4c})	18, 22, 24—27
	—	—	1.899	1.899	$g_{//}$ component of hexa-coordinated Mo^{5+} ($Mo^{5+}_{6c'}$)	18, 22, 24—27
	—	1.883	1.883	1.883	$g_{//}$ component of hexa-coordinated Mo^{5+} (Mo^{5+}_{6c})	18, 22, 24—27
	—	—	1.778	—	$g_{//}$ component of tetra-coordinated Mo^{5+} (Mo^{5+}_{4c})	18, 22, 24—27

temperatures from 373 to 723 K, and decreased rapidly. This reflects the results of TG-DTA, XRD and SA, and strongly correlates with the structural and compositional change in the sample.

Structural Change of Type-I and Formation of Defect Structure.

According to the TG-DTA result, four steps exist by treating Type-I in an oxygen-free atmosphere, as mentioned above.

At the first step (below 500 K), the physically adsorbed water desorbs with a slight amount of weight loss (0.04 wt%), which cause no structural change, and SA remains constant. SA of Type-I is 3.5 $m^2 g^{-1}$ which is larger than that of MoO_3 (1.2 $m^2 g^{-1}$) by three times. It is considered that the increase in SA may be caused by an expansion of the interlayer space between the MoO_6 sheets of MoO_3 by the insertion of protons, as mentioned in the previous paper.[4,7]

For the second step (from 500 to 650 K), the DTA curve shows a very broad endothermic peak at around 550 K with a gradual decrease of 0.81 wt%, which is calculated to be $x = 0.14$ [Fig. 1]. Most of the protons in Type-I are known to be inserted in the intra-layer site of [MoO_6] sheets.[1—5,7,9—13] Therefore, dehydrogenation under an oxygen-free condition results from the intra-layered protons. The proton is removed as H_2O by connecting with the lattice oxygen as $H_xMoO_3 \rightarrow H_{x-x'}MoO_{3-x'/2} + x'/2 \cdot H_2O$. Therefore, this weight loss is due to $x'/2 \cdot H_2O$. The composition changes as $H_{0.25}MoO_3 \rightarrow H_{0.11}MoO_{2.93}$. This composition was calculated from the results of TG-DTA and a chemical analysis. According to the XRD results, Type-I maintains its structure though it removes the lattice oxygen. Therefore, a defect structure, like an oxygen vacancy, is formed. ESR results prove the existence of a defect structure. We call Type-I having a defect structure the "Type-I like structure".

For the third step (from 650 to 723 K), the DTA curve shows a sharp endothermic peak at 664 K, which means a structural rearrangement with dehydrogenation [Fig. 1]. In fact, the components of MoO_2 and MoO_3 show a considerable increase along with a decrease in Type-I, as shown in Fig. 3. The weight loss of 0.71 wt% corresponds to $x = 0.11$ and the composition changes as $H_{0.11}MoO_{2.93} \rightarrow MoO_{2.87}$. The relative intensity of ESR signals increases at this step and takes a maximum at 723 K. A perfect crystalline MoO_3 gives no ESR signal due to Mo^{5+} in theory. However, if MoO_3 has a defect structure, like a vacancy, Mo^{5+} can be detected in the sample. This clearly indicates the existence of a defect structure, such as a vacancy. Therefore, $H_{x-x'}MoO_{3-x'/2}$ should contain a defect. It is reasonable to consider that the increase in SA should result from the formation of a defect structure. We call this the "MoO_3-like structure". Thus, it is concluded that not only Type-I, but also MoO_3, form the Type-I like structure and the MoO_3-like structure.

For the fourth step (above 723 K), Type-I completely disappears and the sample consists of only MoO_2 and MoO_3. The XRD patterns are more sharp and simple, as shown in Fig. 2. It is clearly suggested that the crystallization proceeds at this step, like $MoO_{2.87} \rightarrow 0.87\ MoO_3 + 0.13\ MoO_2$. This shows that the MoO_3-like structure with a defect changes to crystalline MoO_3 without a defect structure. Therefore, SA decreases along with an increase in the treated temperature, because a perfect MoO_3 gives a small SA.

The structural changes in these four steps are shown in Scheme 1.

XANES Study of Type-I. XANES measurement of the total electron yield mode of LMM Auger electrons and low-energy secondary electrons reflect the structure of the surface and/or near to the surface region, because the penetration range into the bulk of the radiation is possibly several tens of angstroms.[28] A Mo L_3-edge XANES study was performed in order to reveal the structure of the surface and near to the surface of Type-I. Figure 8 (I) shows the Mo L_3-edge XANES spectra of the standard materials of Type-I, MoO_3, and MoO_2. The spectra of Type-I and MoO_3 with octahedral symmetry showed two distinct peaks. They are attributed to the electron transition from $2p_{3/2}$ to a vacant 4d state, t_{2g} (d_{xy}, d_{xz}, and d_{yz}) and e_g ($d_{x^2-y^2}$ and d_{z^2}). The peak height of the lower energy side is higher than that of the higher one. This is due to the difference in the transition cross section of the molecular orbital of Mo(4d)–O(2p); theoretically, the intensity is $t_{2g} : e_g = 3 : 2$ for an octahedron. As shown in Fig. 8, the spectrum of Type-I shifted more to the lower

Step 1	Room temperature	⟶	500 K	Dehydration of physically adsorbed water no structural change $H_{0.25}MoO_3$	**Type-I**
Step 2	500 K	⟶	650 K	Dehydrogenation $H_{0.25}MoO_3 \longrightarrow H_{0.11}MoO_{2.93}$	**Type-I like structure**
Step 3	650 K	⟶	723 K	Dehydrogenation $H_{0.11}MoO_{2.93} \longrightarrow MoO_{2.87}$	**MoO_3 like structure** (**Type-I like structure** **MoO_2**)
Step 4	723 K	⟶		Crystallization $MoO_{2.87} \longrightarrow 0.87\ MoO_3 + 0.13\ MoO_2$	**MoO_3 and MoO_2**

Scheme 1. The structural changes of Type-I in oxygen free atmosphere.

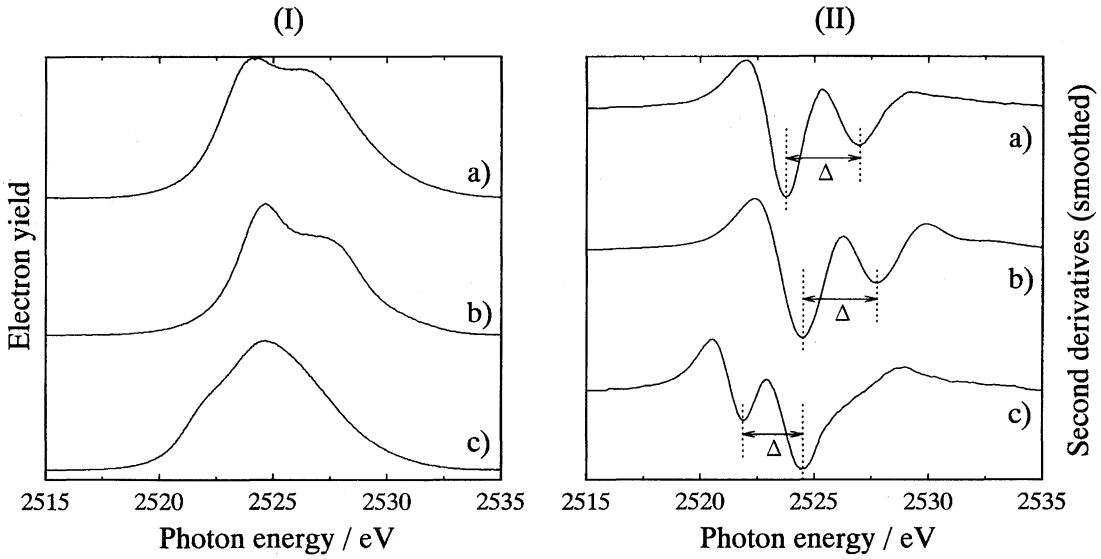

Fig. 8. Mo L_3-edge XANES spectra (I) and the second derivatives (II) of standard materials of a) Type-I, b) MoO_3 and c) MoO_2.

energy side than that of MoO_3. This shift should result from a minor rearrangement of the Mo–O framework of the MoO_6 octahedron, which is caused by the insertion of hydrogen into the intra-layer of MoO_3.[7] Indeed, the hydrogen atoms are stabilized by bonding to the lattice oxygens in the intra-layer.[7] On the other hand, the spectrum of MoO_2 is different from that of Type-I and MoO_3, even though MoO_2 is also constructed from the octahedron. In the molecular orbital of MoO_2, the threefold-degenerate t_{2g} manifold of MoO_6 octahedral symmetry is split into a more stable $d_\perp$ (d_{xy}) orbital and two $d_\perp$ (d_{xz} and d_{yz}) orbitals. The $d_\perp$ orbital overlaps the p_π orbital of the O^{2-} ions, which has three coplanar Mo near neighbors, and the Mo($d_\perp$)–O(p_π)–Mo($d_\perp$) interaction form a quasidegenerate pair of π^* bands. Thus, a pair of Mo 4d electrons in the t_{2g} state occupies a molecular orbital of Mo($d_\perp$)–O(p_π) and the orbital in the e_g state is vacant. Therefore, the peaks may shift more to the lower energy side than that of Type-I and MoO_3, and the peak height of the lower side is smaller than that of the higher one.

The energy gap between the peak-to-peak width (Δ), used as a parameter of the ligand field splitting of the final state 4d orbital, reflects the coordinated environment around the Mo atom. A second derivative of the spectrum is very useful to determine the energy gap.[18,29—33] Figure 8 (II) shows the second derivative of the standard materials. Δ was determined from the second derivative, and summarized in Table 2 along with those of several reference molybdenum compounds.[18,32,33] Δ was determined to be 3.2 eV for Type-I and 3.4 eV for MoO_3, respectively. According to Table 2, the octahedral compounds took Δ =3.1—4.5 eV. It is well understood that the low Δ of Type-I results from a decrease in the energy gap between t_{2g} and e_g of the 4d state by a reduction of Mo ions. Δ of MoO_2, having Mo^{4+} ions, should be smaller than that of a material having Mo^{6+} ions, because of the smaller effect of a perturbation by the ligand field of six O ions. MoO_2 gave Δ =2.5 eV. This value was in good agreement with that of the reported value of 2.4 eV.[33] This result indicates that the reduction of Mo ions leads to a degeneracy of the total 4d state, and makes the energy gap much smaller.

Table 2. The Value of d-Orbital Splitting, Δ, of Molybdenum Compounds
Δ was obtained from the second derivatives.

Sample	Local structure	d-Orbital splitting, Δ / eV
$CoMoO_4$	Octahedral	3.3[32]
MoO_3	Octahedral	3.4*, 4.0,[32] 3.4[33]
H-bronze Type-I	Octahedral	3.2*, 3.1[33]
H-bronze Type-II	Octahedral	3.1[33]
$(NH_4)_6Mo_7O_{24}$	Octahedral	3.6,[32] 2.9[33]
Ba_2CaMoO_6	Octahedral	4.5[32]
MoO_2	Octahedral	2.5*, 2.4[33]
Type-I ($H_{0.25}MoO_3$)*		
Treated temperature	Room temperature	3.2
	373 K	3.2
	473 K	3.1
	523 K	3.2
	573 K	3.2
	623 K	3.2
	673 K	3.1
	723 K	2.2 3.2
	773 K	2.2 3.1
	873 K	2.2 3.1

*: present work.

Figure 9 (I) shows the Mo L_3-edge XANES patterns of Type-I treated at several temperatures in vacuo. All of the spectra looked like that of Type-I and MoO_3. To clarify these spectra, the second derivatives obtained, as shown in Fig. 9 (II). The second derivative above 723 K showed an interesting difference in the peak at around 2522 eV, which should be due to MoO_2, as shown in Fig. 8. Below 673 K the peaks appeared at around 2524 and 2527 eV, and Δ took 3.1—3.2 eV. This is identical with those of Type-I. Above 723 K, the spectrum consists of two component. The peaks appear at around 2522, 2524, 2527 eV and Δ give two values,

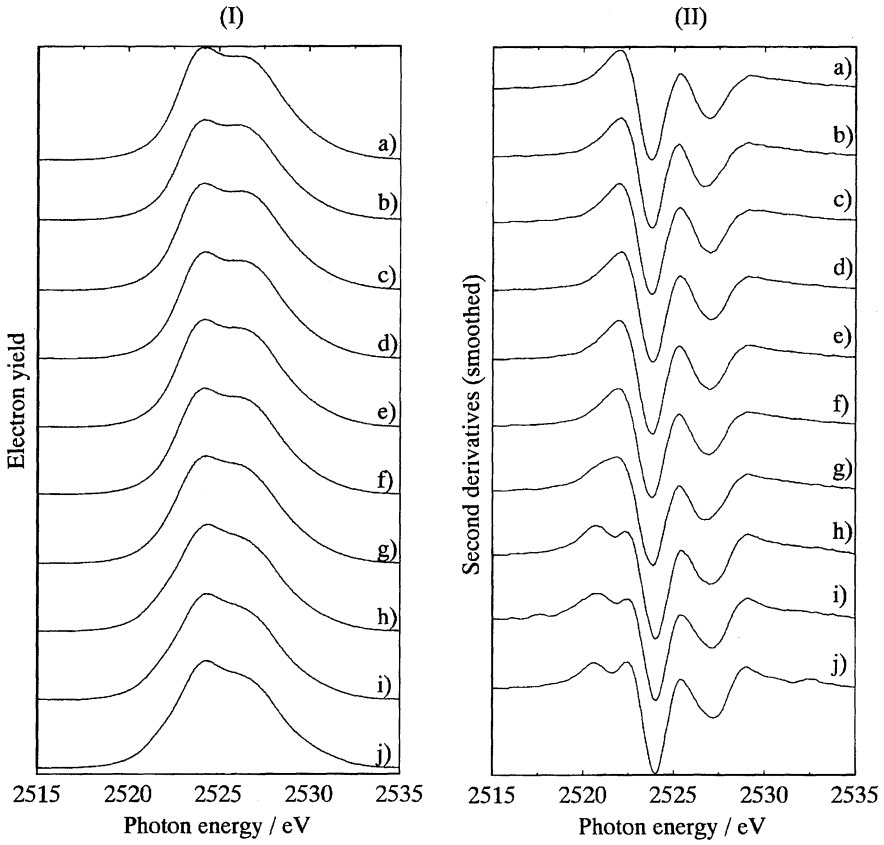

Fig. 9. Mo L_3-edge XANES spectra (I) and their second derivatives (II) of Type-I treated in vacuo at a) room temperature, b) 373 K, c) 473 K, d) 523 K, e) 573 K, f) 623 K, g) 673 K, h) 723 K, i) 773 K, and j) 873 K.

3.1—3.2 eV and 2.2 eV. These just correspond to those of MoO_3 and MoO_2. These results show that the surface of the sample treated above 723 K dominantly consists of MoO_3 and MoO_2.

Catalytic Reaction for Isomerization of 1-Butene on Type-I. Hydrogen molybdenum bronze is expected to be a new functional material as a catalyst. We tried to use it as a catalyst for the isomerization of 1-butene. This reaction is well-known to be a useful method to provide an examination of the catalytic activity and the acidic or basic character of the catalyst. Figure 10 shows the result of a catalytic reaction for isomerization of 1-butene on Type-I treated at various temperatures in vacuo. The reaction proceeded only by isomerization from 1-butene to 2-butene. No other reaction product was not detected. Below 673 K, the conversion from 1-butene to 2-butene increased from 19.5 to 28.5% and the *cis-/trans-* ratio gradually increased from 0.4 to 0.6. Above 673 K, the conversion of 1-butene decreased to 21% and the *cis-/trans-* ratio also decreased to 0.3.

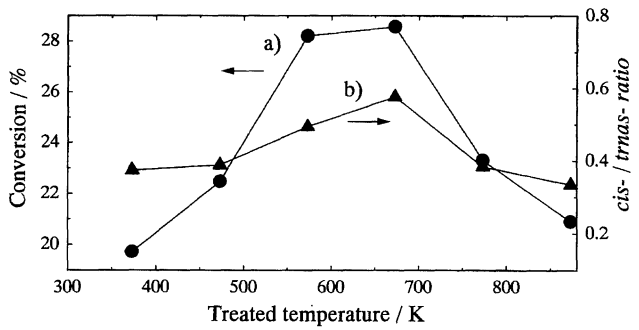

Fig. 10. Isomerization of 1-butene on Type-I treated at various temperatures in vacuo; a) conversation; ●, and b) *cis-/trans-* ratio; ▲.

At the first step (below 500 K), the conversion increases along with an increase in the treated temperature and the *cis-/trans-*ratio remains constant at about 0.4 [Fig. 10]. The *cis-/trans-* ratio shows an indicator for the catalytic active site. In this step, the bulk structure keeps Type-I with no significant change in SA [Figs. 3 and 4]. Since only the physically adsorbed waters are removed, the proton is hardly lost and the defect structure is not appreciably formed. Therefore, the proton can act as an active site for the isomerization of 1-butene, which may be a Brønsted acid. However, a Brønsted acid usually takes about 1 for the *cis-/trans-* ratio.[34] The proton may take on a different behavior from that of the Brønsted acid.

At the second step (from 500 to 650 K), the conversion and *cis-/trans-* ratio increase [Fig. 10]. The proton is released from the Type-I to form the Type-I like structure. The relative intensity of ESR signals due mostly to Mo^{5+}, which consists of hexa- and tetra-coordinated Mo^{5+} coordination state, increases with the decrease in the inserted proton. Moreover, the *cis-/trans-* ratio increases. It is known that the 1-butene isomerization proceeds on the acidic site. The Type-I like structure contains the oxygen vacancies, which show

an acidic property. This can act as an active site for 1-butene isomerization.

At the third step (from 650 to 723 K), the conversion took a maximum at 673 K [Fig. 10]. The bulk structure changes from the Type-I like structure to MoO_2 and the MoO_3 like structure. At the same time, both SA and the relative intensity of ESR signals increase along with an increase in the MoO_3-like structure [Figs. 4 and 7]. These results indicate that the MoO_3-like structure contains a defect, like an oxygen vacancy. The isomerization of 1-butene also proceeds on not only the Type-I like structure, but also on the MoO_3-like structure. The *cis-/trans-* ratio increases from 0.8 to 0.6. This suggests that a new different acidic site appears. This may be another type of vacancy, which results from the MoO_3-like structure.

At the fourth step (above 723 K), the bulk composition brings about crystallization to stoichiometric MoO_3 and MoO_2 [Fig. 2]. The MoO_3 and MoO_2 isomerization of 1-butene hardly takes place. The decrease in the conversion and the *cis-/trans-* ratio may be clearly caused by the progress of crystallization. We could not precisely reveal the catalytic isomerization of 1-butene on Type-I treated at various temperatures in an oxygen-free atmosphere. However, it is clear that the defect structure formed in the Type-I like structure and the MoO_3 like structure play important roles in catalytic isomerization. Further studies concering the catalytic reaction are needed.

References

1) O. Glemser and G. Lutz, *Z. Anorg. Allg. Chem.*, **264**, 17 (1951); **269**, 93 (1952); **285**, 173 (1956).

2) K. A. Wilhelm, *Acta. Chem. Scand.*, **23**, 419 (1969).

3) F. A. Schröder and H. Weitzel, *Z. Anorg. Allg. Chem.*, **435**, 247 (1977).

4) J. J. Birtill and P. G. Dickens, *Mater. Res. Bull.*, **13**, 311 (1978).

5) R. C. T. Slader, T. K. Halstead, and P. G. Dickens, *J. Solid State Chem.*, **34**, 183 (1980).

6) G. C. Bond and J. B. P. Tripathi, *Trans. Faraday Soc.*, **72**, 933 (1976).

7) N. Sotani, K. Eda, and M. Kunitomo, *Trends Inorg. Chem.*, **1**, 23 (1991).

8) P. G. Dickens, J. J. Birtill, and C. J. Wright, *J. Solid State Chem.*, **28**, 185 (1979).

9) N. Sotani, M. Kunitomo, and M. Hasegawa, *Chem. Lett.*, **1983**, 647.

10) N. Sotani, N. Yoshida, Y. Kawamoto, S. Kishimoto, and M. Hasegawa, *Bull. Chem. Soc. Jpn.*, **57**, 3032 (1984).

11) N. Sotani, Y. Kawamoto, and M. Inui, *Mater. Res. Bull.*, **18**, 797 (1983).

12) N. Sotani, N. Yoshida, Y. Yoshioka, and S. Kishimoto, *Bull. Chem. Soc. Jpn.*, **58**, 1626 (1985).

13) T. Ohno, H. Miyata, F. Hatayama, and N. Sotani, *Bull. Chem. Soc. Jpn.*, **60**, 3435 (1987).

14) Cl. Ritter, W. Müller-Warmuth, and R. Schöllhorn, *J. Chem. Phys.*, **83**, 6130 (1985).

15) N. Sotani and M. Hasegawa, *React. Kinet. Catal. Lett.*, **31**, 65 (1986).

16) K. Eda, *J. Mater. Chem.*, **2**, 533 (1992).

17) C. Choain and F. Marion, *Bull. Soc. Chim. Fr.*, **1963**, 212.

18) K. Nakamura, K. Eda, N. Sotani, and S. Hasegawa, to be submitted.

19) K. D. Bowers and J. Owen, *Rep. Prog. Phys.*, **18**, 304 (1955).

20) R. J. Kokes, "Experimental Methods in Catalytic Research," ed by R. B. Anderson, Academic Press, New York (1968), pp. 436—475.

21) J. H. E. Griffiths, J. Owen, and I. M. Ward, *Proc. R. Soc., Ser. A*, **219**, 526 (1953).

22) K. Dyrek and M. Labanowska, *J. Chem. Soc., Faraday Trans.*, **87**, 1003 (1991).

23) H. Lunsford and J. P. Jayne, *J. Chem. Phys.*, **44**, 1487 (1966).

24) M. Che, F. Figueras, M. Forissier, J. C. McAteer, M. Perrin, J. I. Portefaix, and H. Praliaud, "Proc. VIth Int. Congr. Catal.," The Chemical Society, London, 1977, Abstr., Vol. 1, p. 261.

25) R. F. Howe and I. R. Leith, *J. Chem. Soc., Faraday Trans. 1*, **69**, 1967 (1973).

26) C. Louis and M. Che, *J. Phys. Chem.*, **91**, 2875 (1987).

27) A. Latef, C. F. Aissi, and M. Guelton, *J. Catal.*, **119**, 368 (1989).

28) A. Erbil, G. S. Cargill, R. Frahm, and R. F. Boehme, *Phys. Rev. B*, **37**, 2450 (1988).

29) J. Evans, W. Frederick, and W. Mosselmans, *J. Phys. Chem.*, **95**, 9673 (1991).

30) G. N. George, W. E. Cleland, J. H. Enemark, B. E. Smith, C. A. Kipke, S. A. Roberts, and S. P. Cramer, *J. Am. Chem. Soc.*, **122**, 2541 (1990).

31) H. Hu, I. E. Wachs, and S. R. Bare, *J. Phys. Chem.*, **99**, 10897 (1995).

32) S. R. Bare, G. E. Mitchell, J. J. Maj, G. E. Vrieland, and J. L. Gland, *J. Phys. Chem.*, **97**, 6048 (1993).

33) H. Aritani, T. Tanaka, T. Funabiki, S. Yoshida, N. Sotani, K. Eda, and S. Hasegawa, *J. Phys. Chem.*, **100**, 19495 (1996).

34) K. Tanabe, "Acts of Catalyst," Kagakudojin, Tokyo (1974), p. 21.